Experimental characterization of the multiaxial dynamic behavior of a nickel-titanium shape memory alloy

P. QUILLERY[a], B. DURAND[a], O. HUBERT[a], H. ZHAO[a,b]

a. LMT (ENS Paris-Saclay, CNRS, Université Paris-Saclay) / CNRS, 61 avenue du Président Wilson 94235 Cachan, France, quillery@lmt.ens-cachan.fr

b. UFR Ingénierie, Université Pierre et Marie Curie, Sorbonne Universités, Paris, zhao@lmt.ens-cachan.fr

Abstract :

The multiaxial behaviour of a nickel-titanium shape memory alloy (SMA) is experimentally studied. Indeed the solid-solid phase transformation that occurs with stress induces a complex behavior, depending on the loading parameters such as the deformation rate or the multiaxial character of the loading. The solid-solid transformation can be initiated by stresses or thermal loading. In this work, the pseudo-elastic behavior is measured for an equi-biaxial compression loading situation thanks to a home made impact testing set-up and Hopkinson split bars. Measurements are conducted by the use of high speed infrared and optical cameras and a Hopkinson bar set-up. The strain field is estimated by digital image correlation and stresses in the central area of specimen are estimated from boundary conditions through informations given by strain gauges placed on the bars. The strain appears homogeneous in the biaxial loading region of interest and a significant rise in temperature is observed.

Keywords : Multi-axial testing, dynamic testing, shape memory alloys (SMA)

1 Introduction

The measurement of mechanical behavior of materials submitted to biaxial loading is necessary for the identification or validation of models. The bi-axial tests are relatively well controlled and very often used in quasi-static conditions. However, dynamic bi-axial tests remain infrequent and are often difficult to carry out and analyze.

The setting up of biaxial tests is justified by the complexity of some behaviors. For instance, in the case of a simple Von-Mises threshold combined with isotropic hardening, the yield surface is not symmetrical in the principal stress plane. To ensure a perfect identification of the yield stresses, controlled multiaxial tests are thus necessary. In the case of anisotropic materials, these tests are even more relevant to define the yield surfaces and hardenings. Shape memory alloys exhibit a very complex and non-symmetrical yield surface, as shown by K. Lavernhe Taillard [1]. In this former study, the transformation surface of a CuZnAl SMA has been identified. Non proportional effects (strain depends on stress path) have been clearly highlighted.

For many materials, the mechanical behavior also depends on the strain rate. Visco-plastic materials, architectured foams or shape memory alloys can be given as classical examples. Stiebler and al. [2] and Kraiem [3] has shows in their studies the strain rate dependence of the yield surface evolution. Modifications being not homothetic, multiaxial characterization at different strain rates are very relevant for identification or validation of models. In this way, many studies are conducted to carry out multiaxial dynamic tests. Because of the necessity of a perfect time synchronization between several short loading waves, this kind of test remains complex to manage. The most explored way consists in separating an unique incident wave in different waves intended for different axes. The time shifting between the generated loading waves is therefore reduced.

2 Multi-axial dynamic sets-ups

Exploratory tests in biaxial dynamics began with simple stress states. The combination of an axial tensile or compressive stress and a shear stress are then the first tests that show that conducted to biaxial loadings. These tests are often associated with classical Hopkinson bars. Although

the impact is easy to generate, the measurement is difficult because the combination of both solicitations is hard to dissociate at the output.

2.1 Shear and normal stresses

The set-up presented in the article written by Lewis et al. [4] describes a system of compression and torsion loadings. The torsional loading is applied by a torsionally prestressed bar and locked by a brake. When the system is triggered, the brake is released and the preloaded bar solicits the torsional sample. To ensure a good synchronization, the brake is released by a detonation, and the detonation is controlled by the compression bar. Knowing the velocities of waves, which are not different in case of compression or torsion, and the path followed by of each of them, Lewis's device enables for a synchronization up to $\pm 10\mu s$.

Stiebler et al. [2] present in their study a combined torsion-tension system. The loading is carried out by a previously constrained bar and by a brake pressure applied at the bar end, near the sample. When the brake is suddenly released, the energy stored in the bar, composed on the one hand by a torsion energy, and by a tension energy on the other hand is then released. The inertia of the bars makes it possible to load the sample.

Another study [5] presents a complex loading in dynamics. Pure shear loading is performed by using a set-up especially designed for this application and adapted to a classical Hopkinson bar system. The parts of plates between the two jaws are solicited in pure shear.

The set-up presented in the Rittel's study [6] uses a unique impact for compression and shear loading. Adapted to a conventional uni-axial Hopkinson split bar system, two pieces with inclined planes enable for a combined shear-compression loading. Shear and compression loadings are proportional and varying the angle of planes changes the proportionality ratio. By this method they can dissociate the two loading parts.

In the publication of Hou and al. [7] or Tounsia and al. [8], the exploration of a combined loading in shear and compression is also presented. The inclined plane assembly is, this time, confined and the translation of these parts relatively to the bars is therefore not allowed.

2.2 Confined testing

Grolleau [9] explores the path of a complex solicitation by putting a membrane submitted to a dynamic pressure. The latter fixed on a the output bar undergoes isostatic compression applied via the input bar and a fluid cavity. The analysis by the strain gauges makes it possible to determine the pressure applied to the membrane.

The researches of Albertini [10] and Bailly [11] explored the confinement. By confining the sample in the transverse direction with a rigid system, the loading along the longitudinal axis induces, by Poisson effect, a compression in the transverse direction. Containment can be achieved by a pressurized fluid cavity system or by rigid mechanical parts. Here again, it is difficult to estimate the stress amplitude. By knowing the Poisson's ratio, we can calculate the respective loads.

2.3 Multi-impacts

In the 1980s, Albertini [12] proposed a biaxial tension system with preloaded cables and explosive charge released brakes. The use of explosive charges allows a good synchronization because the triggering is brief. The ratio between both loading directions can be chosen.

Hummeltenberg [13] presented a biaxial compression test with two separated impactors. Synchronization is difficult to achieve despite the use of electronic triggers .

In the next section a system allowing, from a single impactor, to apply a multiaxial loading thanks to an innovating mechanical set-up is detailed

3 A new experimental set-up for multi-axial dynamic testing

In the range of dynamic testing, we focused on split Hopkinson bar systems (figure 1), which allow strain rates from $10/s$ to $100/s$ [14] to be reached. An home-made set-up has been developed and adapted to such a single split system in order to perform equi-biaxial compression.

The material constitutive of the bars is known and used in the range of elasticity, so that the system is considered as test body of measurement chain. Signals from gauges can be separated into three parts in the classical testing resolution (and into four parts in our case) : (i) the incident

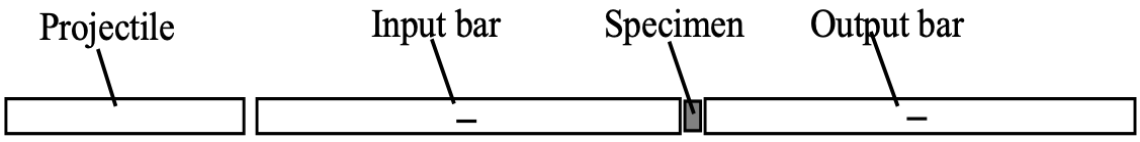

FIGURE 1 – Classical uni-axial split Hopkinson bar set-up

strain wave that is imposed in the input bar by projectile impact, (ii) the reflected strain wave which is the response of the specimen into the input bar, (iii) the transmitted strain wave which is the response of the specimen into the output bar, (figure 2). Obtaining these three signals that propagate in the bars from strain gauges makes it possible to determine the forces and the velocities at the interfaces between the bars and the sample, and thus to determine its stress and strain state during the test.

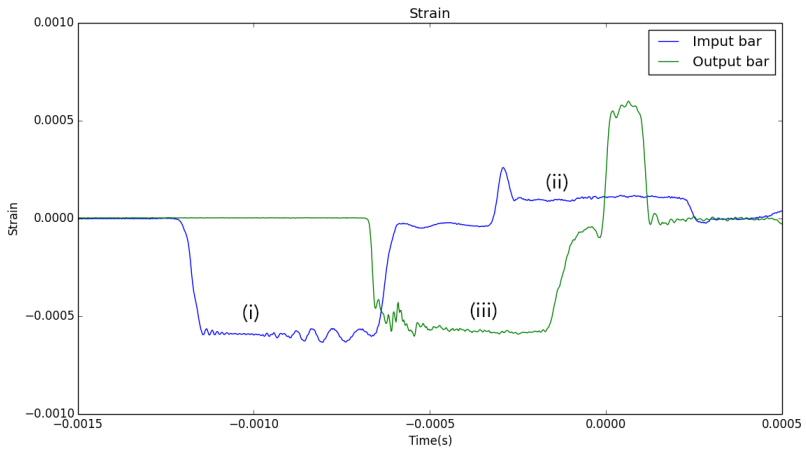

FIGURE 2 – Typical strain waves measured on a Hopkinson set-up

The biaxial compression set-up (figure 3) fits with a classical Hopkinson bar bench. The forces in the sample along both longitudinal and transverse directions are measured by using the gauges glued on the coaxial output bars. The set-up includes 45° angle pieces that transmit the incident wave to the sample along the transverse direction. The transverse force in the sample is generated by the inertia of the external bar and the longitudinal force is generated by the internal bar inertia.

The Hopkinson formulae [14] enable the determination of the forces at the interfaces between the bars and sketched in figure 3. Knowing the friction coefficient in the mechanism, it is possible to evaluate the longitudinal and transversal forces at the boundary of the sample. Stress

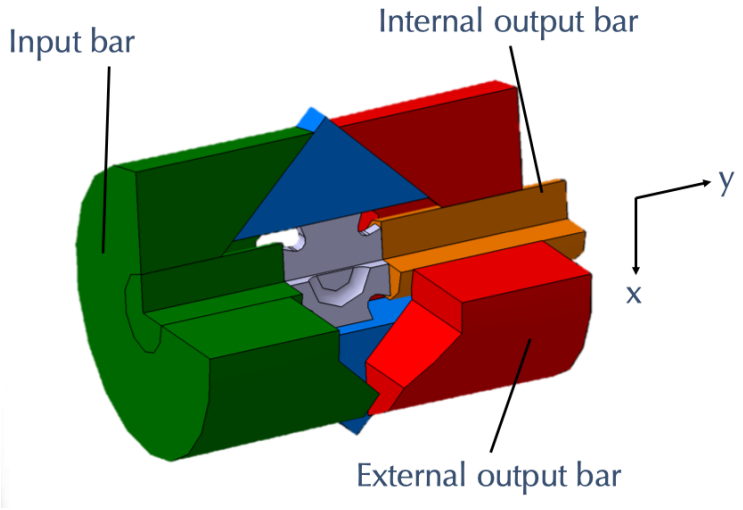

FIGURE 3 – Schematic of the set-up

state in the area of interest is calculated from these forces using an elastic finite element calculation.

Gauges are glued on the input and on the two output bars to measure strains thanks to usual Wheatstone bridge facilities (recording frequency is 500 KHz). The knowledge of the measurement chain parameters is useful for strain, force and velocity calculations. The gain of each gauge is therefore properly measured thanks to a force sensor during preliminary static tests.

$$F_{imput}(t) = S_B E(\epsilon_i(t) + \epsilon_r(t)) \qquad and \qquad V_{input}(t) = C_0(e_i(t) - e_r(t)) \tag{1}$$

$$F_{output_{ext}}(t) = S_B E\epsilon_{t_{ext}}(t) \qquad and \qquad V_{output_{ext}}(t) = C_0\epsilon_{t_{ext}}(t) \tag{2}$$

$$F_{output_{int}}(t) = S_B E\epsilon_{t_{int}}(t) \qquad and \qquad V_{output_{int}}(t) = C_0\epsilon_{t_{int}}(t) \tag{3}$$

S_B, E and C_0 are the bar cross-sectional area, Young modulus, and elastic wave celerity respectively. ϵ_i is the incident deformation, ϵ_r the reflected deformation, $\epsilon_{t_{int}}$ the input transmitted wave and $\epsilon_{t_{ext}}$ the output transmitted deformation.

The specimen is designed to concentrate stresses in a region of interest (ROI). This ROI is a $3\,mm$ diameter circle with a $0.5\,mm$ thickness, the external part of the specimen is $2\,mm$

thickness. The maximum overall dimension is fixed by the Hopkinson bar system and the biaxial set-up. The external dimensions of the specimen are $8\,mm \times 8\,mm$, the cruciform geometry is shown in figure (4a).

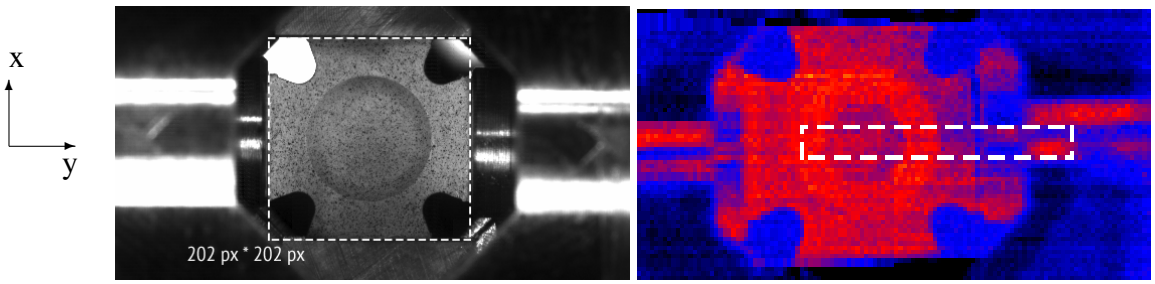

(a) Reference image and area for DIC (b) Observation zone for a 15000 Hz infrared recording ($64\,px \times 8\,px$)

FIGURE 4 – Optical and thermal image settings

The specimen has been designed after a finite element pre-simulation using a non-linear behavior close to the expected behavior. The designed shape avoids buckling and optimizes the stress concentration. Buckling is more restrictive in statics than in dynamics because of the inertia, the parametric finite element analysis is thus realized in quasi-statics condition and verified in dynamic condition. From the measured forces we can calculate the stresses in the ROI by the finite element modeling.

$$\begin{pmatrix} \overline{\sigma_{xx}} \\ \overline{\sigma_{yy}} \end{pmatrix} = \begin{pmatrix} m_{xx} & m_{xy} \\ m_{yx} & m_{yy} \end{pmatrix} \begin{pmatrix} F_x \\ F_y \end{pmatrix} \tag{4}$$

The experiment is multi-instrumented to access on many parameters : the bi-axial specimen is tracked by a high speed numerical camera to accurately calculate the strain field by digital image correlation (DIC). The recording is realized by a SA5 fast-camera at 50000Hz and on a 512px $\times$ 271px area. DIC principle consists of calculating the difference between two images, a reference one and a distorted one, assuming the conservation of the brightness level in spite of a possible heterogeneous lightening. Several high-power lights have been arranged in such a way that a homogeneous luminosity during the test can be considered. An image is seen numerically as a matrix function characterizing the gray level of each pixel. If we call x the position, f a function of representing the reference image and g a function representing the deformed image,

the determination of the displacement field u is obtained by minimizing the residue formed by the square of the left-hand term in equation (5).

$$f(x) - g(x + u(x)) = 0 \tag{5}$$

Correlation code Correli-RT3 has been used considering the displacement field as continuous. This code allows the identification of the displacement on each node of a finite element mesh composed of 3-nodes triangular elements. The obtained displacement is regularized by an elastic solution [15].

To complete these measurements, a an Infra-Red camera is placed in front of the other side of the sample which has been painted in black in order to assume the ROI emissivity as a constant. The measurement of thermal field is crucial especially for SMA because the austenite to martensite transformation is accompanied by a strong heat release due to latent heat effect (transient temperature increase of about 40°C for the studied material) The way this transformation takes place will give us information about the transformation rate that is a crucial point in the behavior. A calibration of the infrared sensor with a black body enables the link between the digital level measured by the camera and the temperature to be obtained. Figure (4b) shows the full range calibration and the restricted area chosen to increase the recording frequency to 15000 Hz. This observation area, of about 64×8 pixels, enables to track the specimen during the test and to compensate the rigid body displacement. Only a small part of the ROI is observed by the infrared camera at 15000 Hz, this part appears homogeneous in temperature, so that a uniform heating is considered in the whole ROI.

4 Experimental results

From informations given by the three gauges, figure 5a shows the calculated strains as a function of time.

After time shifting to virtually transport the signals from the strain gauges to the multi-axial set-up interfaces, and after Hopkinson formulae application, we can calculate the forces and the velocities at the interfaces (figures 5b and 5c). We have then to check the equilibrium of

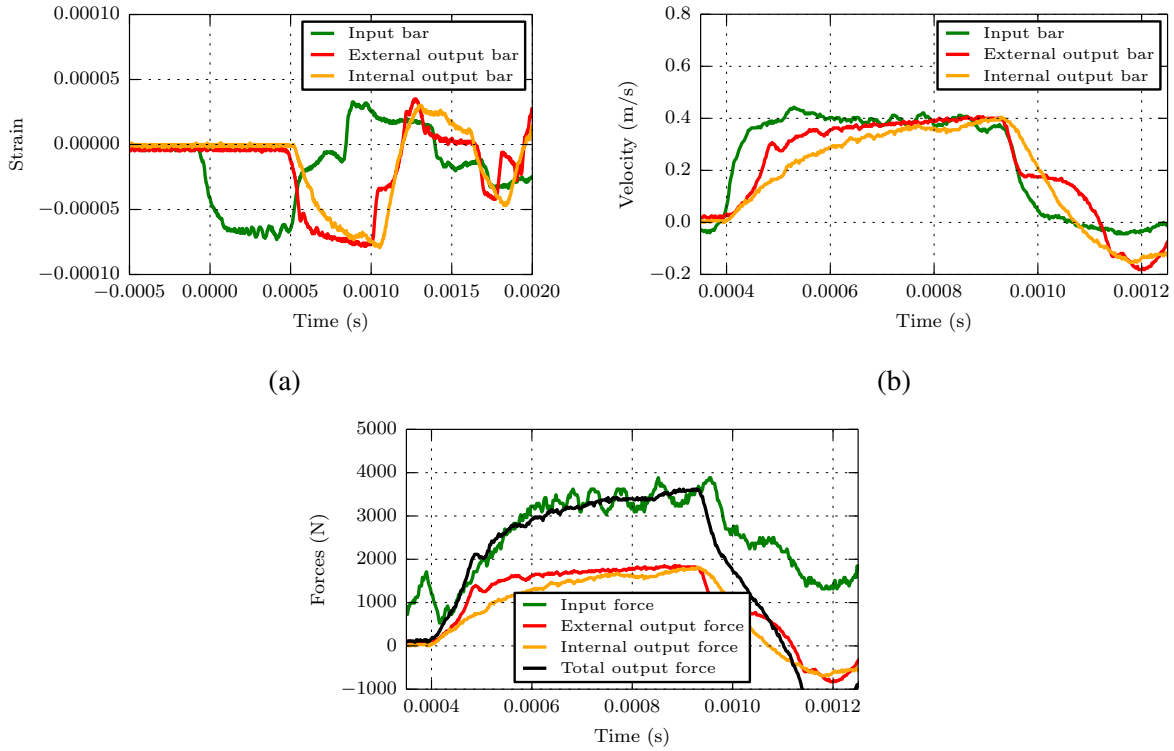

(a) (b)

(c)

FIGURE 5 – Quantities calculated from gauge measurements

the input bar force and of the total output bar force [16]. Figure 5c confirms that the balance is preserved. A steady state is also reached because all velocities are equal.

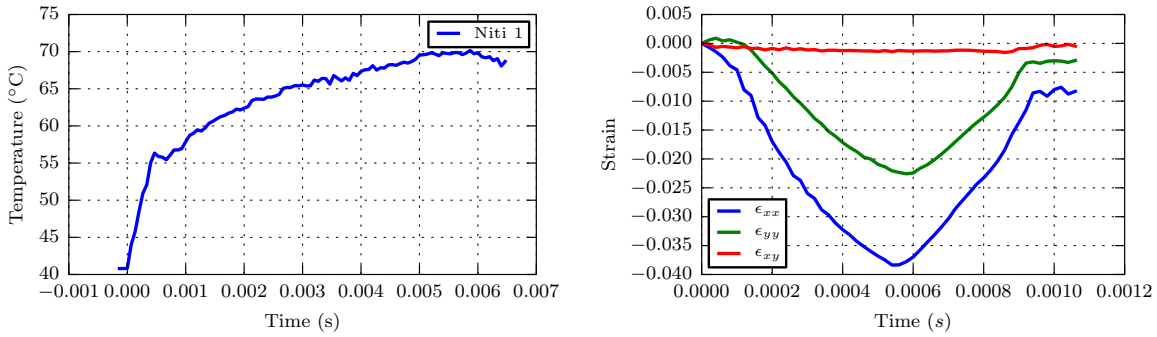

(a) Temperature evolution in ROI (b) Strains calculated by DIC in the ROI

FIGURE 6 – Measurements from IR and fast cameras

However we observe that the force in the internal output bar is a few lower than the force in the external one. This difference can be explained by the friction at the sliding interfaces of the biaxial set up, higher along the x (transverse) direction than along the y (longitudinal) direction. So we have to considere a friction ratio determined thank's to previous experiments

carried out using isotropic aluminum cruciform specimen. The friction coefficient has been roughly estimated to 0.03, which is consistent with smooth lubricated steel surfaces [17].

Average stress components σ_{xx} and σ_{yy} are calculated form the transverse and longitudinal forces F_x and F_y thanks to equation (4) (Parameters of matrix m_{ij} are : $m_{xx} = m_{yy} = 0.2941\,mm^{-2}$ and $m_{xy} = m_{yx} = -0.0794\,mm^{-2}$). Average strain components ϵ_{xx}, ϵ_{yy} and ϵ_{xy} are calculated in the ROI from DIC measurements. ϵ_{xx} and ϵ_{yy} are plotted as function of time in figure 6b. Strains do not seem perfectly synchronized. The lower magnitude of ϵ_{yy} and ϵ_{xx} are in accordance with the lower stress level along y axis (figure 8a, NiTi1). This difference is explained by unwanted clearances which delay the loading arrival. At the beginning, the strain along y can be related to a Poisson effect. By this calculations and Von-Mises eq. (6) and (7) criterion asumption, we can plot equivalent behavior for biaxial condition of the tested specimen (figure 7).

$$\sigma_{VM} = \sqrt{\frac{1}{2}\left(\left(\sigma_{xx} - \sigma_{yy}\right)^2 + \sigma_{xx}^2 + \sigma_{yy}^2\right)} \tag{6}$$

$$\epsilon_{LV} = \sqrt{\frac{2}{3}\left(\epsilon_{xx}^2 + \epsilon_{yy}^2 + 2\epsilon_{xy}^2\right)} \tag{7}$$

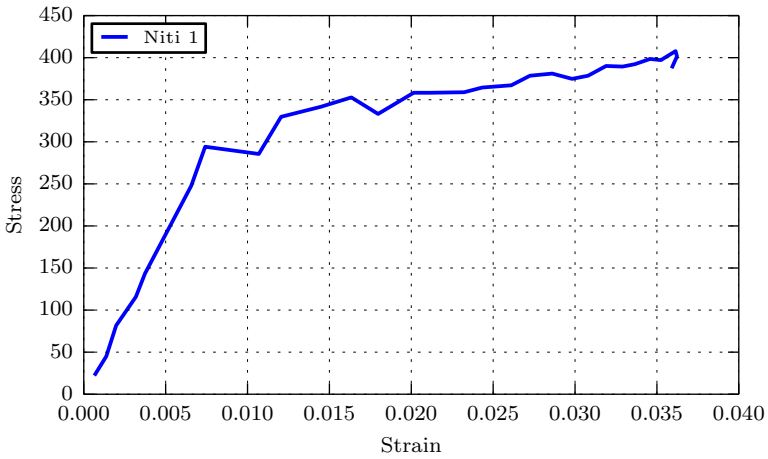

FIGURE 7 – Von-Mises mechanical behaviour

At the end, the strain has reached a deformation of about 3.5%. The infrared observations allow us to calculate the temperature rise during the test. Figure 6a shows a brutal increase during the

first $1ms$. showing that temperature is increasing at the very beginning of the test. However, it must be noticed that the temperature increases along a time range (about 6ms) much longer than the duration of mechanical loading (lower than 1ms).

All these observations will allow us to to improve the modeling of these materials, using for example the proposition of [18].

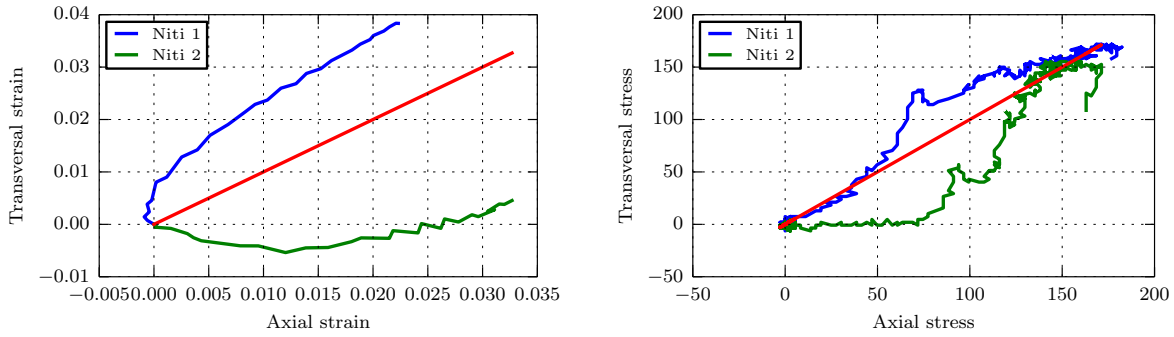

(a) Axial strain by transversal strain

(b) Axial stress by transversal stress

FIGURE 8 – Multiaxiality ratio for the two specimens

Several tests were conducted on specimens machined in the same material. We thus tried to evaluate the reproducibility of the tests. Figures 8a and 8b show the axial paths followed during the two performed tests in terms of deformation and stress. Even if the two curves are different and do not correspond to the expected loading path shown in red, the equivalent behavior appears repeatable as shown on figure 9 leading to a kind of intrinsic sensitivity to the loading rate.

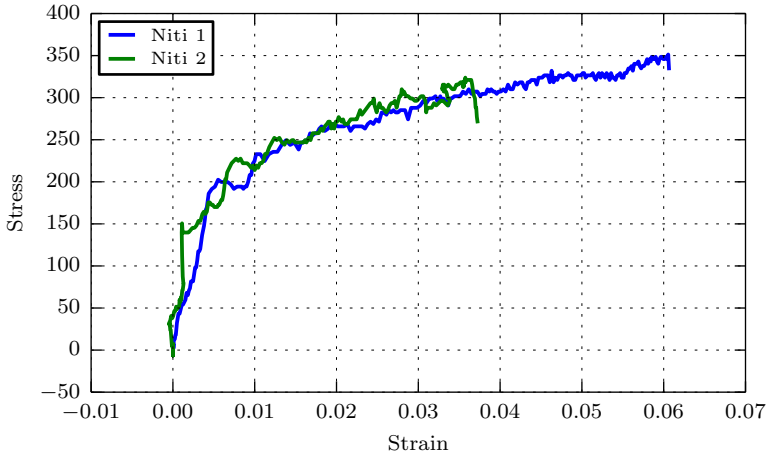

FIGURE 9 – Sum of strains by sum of stresses

5 Conclusion

This study presents results obtained from a new set-up for dynamic multiaxial tests. The improvements to this system that can be expected are a better synchronization of the longitudinal and transverse loadings on the one hand and a better control of the loading ratio on the other hand by a better knowledge of friction coefficient. Multi-instrumentation allows accurate measurements of the loading : strain and temperature fields. This information is necessary for the characterization of complex materials such as shape memory alloys, exhibiting a strong chemo-thermo-mechanical coupling.

Références

[1] K. Lavernhe Taillard, S. Calloch, S. Arbab-Chirani, and C. Lexcellent, "Multiaxial Shape Memory Effect and Superelasticity," *Strain*, vol. 45, no. 1, pp. 77–84, 2009.

[2] K. Stiebler, H.-D. Kunze, and E. El-Magd, "Description of the flow behaviour of a high strength austenitic steel under biaxial loading by a constitutive equation," *Nuclear Engineering and Design*, vol. 127, pp. 85–93, May 1991.

[3] O. Kraiem, M. Houillon, N. Schmitt, and H. Zhao, "Caractérisation et modélisation du comportement mécanique d'une mousse fragile," p. 7, 2015.

[4] J. L. Lewis and W. Goldsmith, "The dynamic fracture and prefracture response of compact bone by split Hopkinson bar methods," *Journal of Biomechanics*, vol. 8, pp. 27–40, Jan. 1975.

[5] G. Gary and W. Nowacki, "Essai de cisaillement plan appliqué à des tôles minces," *Journal de Physique IV Colloque*, vol. 04, no. C8, pp. C8–65–C8–70, 1994.

[6] D. Rittel, S. Lee, and G. Ravichandran, "A shear-compression specimen for large strain testing," *Experimental Mechanics*, vol. 42, pp. 58–64, Mar. 2002.

[7] B. Hou, S. Pattofatto, Y. Li, and H. Zhao, "Impact behavior of honeycombs under combined shear-compression, Part analysis," *International Journal of Solids and Structures*, vol. 48, p. 698, Mar. 2011.

[8] R. Tounsi, E. Markiewicz, G. Haugou, F. Chaari, and B. Zouari, "Dynamic behaviour of honeycombs under mixed shear-compression loading : Experiments and analysis of combined effects of loading angle and cells in-plane orientation," *International Journal of Solids and Structures*, vol. 80, pp. 501–511, Feb. 2016.

[9] V. Grolleau, G. Gary, and D. Mohr, "Biaxial Testing of Sheet Materials at High Strain Rates Using Viscoelastic Bars," *Experimental Mechanics*, vol. 48, no. 3, pp. 293–306, 2008.

[10] C. Albertini, E. Cadoni, and G. Solomos, "Advances in the Hopkinson bar testing of irradiated/non-irradiated nuclear materials and large specimens," *Philosophical Transactions of the Royal Society A : Mathematical, Physical and Engineering Sciences*, vol. 372, pp. 20130197–20130197, May 2014.

[11] P. Bailly, F. Delvare, J. Hanus, J. Vial, M. Biessy, and D. Picart, "Dynamic behavior of an aggregate material at simultaneous high pressure and strain rate : SHPB triaxial tests.," *International Journal of Impact Engineering*, vol. 38, no. 2-3, pp. 73–84, 2011.

[12] C. Albertini and M. Montagnani, "Dynamic uniaxial and biaxial stress-strain relationships for austenitic stainless steels," vol. Volume 57, pp. 107–123, 1980.

[13] A. Hummeltenberg and M. Curbach, "Entwurf und Aufbau eines zweiaxialen Split-Hopkinson-Bars," *Beton- und Stahlbetonbau*, vol. 107, no. 6, pp. 394–400, 2012.

[14] B. Hopkinson, "A method of measuring the pressure produced in the detonation of high explosives or by the impact of bullets," *Philosophical Transactions of the Royal Society of London. Series A, Containing Papers of a Mathematical or Physical Character*, vol. 213, pp. 437–456, 1914.

[15] F. Hild, A. Bouterf, P. Forquin, and S. Roux, "On the Use of Digital Image Correlation for the Analysis of the Dynamic Behavior of Materials," in *The Micro-World Observed by Ultra High-Speed Cameras*, pp. 185–206, 2018.

[16] H. Zhao and G. Gary, "On the use of SHPB techniques to determine the dynamic behavior of materials in the range of small strains," *International Journal of Solids and Structures*, vol. 33, pp. 3363–3375, Sept. 1996.

[17] B. Durand, A. Zouari, H. Zhao, and P. Quillery, "Biaxial Compression Tests on Hopkinson Bars," in *The 18th European International Conference on Experimental Mechanics (ICEM18)*, vol. 2 of *The 18th European International Conference on Experimental Mechanics (ICEM18)*, (Bruxelles, Belgium), p. 420, July 2018.

[18] A. Maynadier, D. Depriester, K. Lavernhe-Taillard, and O. Hubert, "Thermo-mechanical description of phase transformation in Ni-Ti Shape Memory Alloy," *Procedia Engineering*, vol. 10, pp. 2208–2213, 2011.